Spectral diversity allows remote detection of the rehabilitation status in an Amazonian iron mining complex

Markus Gastauer, Wilson R Nascimento, Cecílio Frois Caldeira, Silvio Junio Ramos, Pedro Walfir M. Souza-Filho, Jean-Baptiste Féret

International Journal of Applied Earth Observations and Geoinformation 106 (2022) 102653

Contents lists available at ScienceDirect

International Journal of Applied Earth Observations and Geoinformation

journal homepage: www.elsevier.com/locate/jag

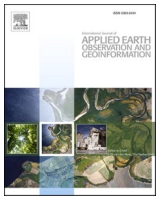

Spectral diversity allows remote detection of the rehabilitation status in an Amazonian iron mining complex

Markus Gastauer [a,*], Wilson R. Nascimento Jr. [a], Cecílio Frois Caldeira [a], Silvio Junio Ramos [a], Pedro Walfir M. Souza-Filho [a], Jean-Baptiste Féret [b]

[a] Instituto Tecnológico Vale, R. Boaventura da Silva, 911, CEP 66055-090, Bairro Nazaré, Belém, Pará
[b] UMR-TETIS, IRSTEA Montpellier, Maison de la Télédétection, 500 rue Jean-François Breton, 34093 Montpellier Cedex 5, France

ARTICLE INFO

Keywords:
Carajás National Forest
Sentinel-2 mission
Environmental assessments
Remote sensing
successional advancement

ABSTRACT

Mineland rehabilitation is intended to reduce the overall impacts of mining on biodiversity and ecosystem services and requires periodic monitoring to guarantee institutional tractability and to refine rehabilitation practices. As time- and money-consuming field surveys challenge this monitoring, the aim of this study was to develop a remote sensing framework to assess the environmental quality of minelands undergoing rehabilitation based on free and open-access multispectral Sentinel-2 images. For this purpose, we linked spectral diversity, i.e., measures of spectral variation among neighboring pixels, to the field-surveyed environmental quality of a rehabilitation chronosequence covering five waste piles in the Carajás National Forest, Eastern Amazon. Field data were separated into a training data set from 2017 (54 plots) and a testing data set from 2019 (66 plots). Based on the training data set, we optimized the computational parameters of spectral diversity (separation of vegetated from nonvegetated pixels by the normalized difference vegetation index [NDVI], size of the buffer zones, number of clusters representing distinct spectral species and applied diversity metrics), maximizing the accuracy of the remote monitoring approach. Then, we validated the procedure with the testing data set and compared the number of areas undergoing rehabilitation and their quality from 2017 and 2019. The overall accuracy of our methodology was 83%, and user and producer accuracies exceeded 60% for all rehabilitation classes, enabling the remote sensing of successional advancement of rehabilitating minelands. Despite punctual losses in spectral diversity, we detected comprehensive gains in spectral diversity within the target structures. This is due to an increase in the overall rehabilitation area from 282.39 to 364.54 ha, but enhancements in the spectral diversity of already vegetated areas indicate the successional advancement of these areas with time, reducing the overall impact of mining activities on biodiversity and ecosystem services. We conclude that the remote sensing framework presented here is promising for mapping environmental quality in minelands undergoing rehabilitation, and we encourage its integration in current monitoring protocols to reduce costs and increase the transparency of a company's rehabilitation activities, as freely available satellite images and open-source software are applied.

1. Introduction

By restituting species communities, vegetation structure and ecological processes as far as possible to predisturbance levels (Gastauer et al., 2018; Wortley et al., 2013), mineland rehabilitation is intended to reduce the overall impacts of mining on biodiversity and ecosystem services (Perring et al., 2015; Gann et al., 2019; Guerra et al., 2020). Monitoring this process is indispensable to guarantee the corporate tractability of such mineland rehabilitation activities (Gastauer et al., 2018; Lamb et al., 2015; Latawiec and Agol, 2016), track environmental advances in these areas (Gastauer et al., 2019), refine rehabilitation practices and attain true ecological rehabilitation (Gastauer et al., 2018; Mazón et al., 2019; Lechner et al., 2018). The environmental quality of rehabilitating minelands, i.e., the degree to which ecological attributes recover toward predisturbance levels, is commonly measured as enhancements in vegetation structure, community diversity and ecological processes (Wortley et al., 2013; Ruiz-Jaén and Aide, 2005). It is estimated as the proportion to which rehabilitating sites converge to the

* Corresponding author.
E-mail address: markus.gastauer@itv.org (M. Gastauer).

https://doi.org/10.1016/j.jag.2021.102653
Received 20 September 2021; Received in revised form 2 December 2021; Accepted 11 December 2021
Available online 16 December 2021

reference sites after ordinating degraded areas, rehabilitating sites and reference ecosystems based on field-surveyed ecosystem characteristics using multivariate approaches (Fig. 2A) (Gastauer et al., 2020a). Despite high reliability, this procedure requires extensive field sampling and is thus timely and spatially limited by technical expertise, high costs and low possibilities for automatization, and upscaling is required to monitor increasing amounts of rehabilitating minelands (Sonter et al., 2020).

The increasing availability of high-resolution satellite imagery, supported by technological, computational, and modeling advances, provides data on the optical properties of the Earth's surface over unprecedented spatial and temporal scales (Martin, 2020; de Almeida et al., 2020). This information opens perspectives for a wide range of applications in ecology (Kerr and Ostrovsky, 2003; Lechner et al., 2020), including environmental monitoring activities (Johansen et al., 2019). With the use of geographic object-based image analysis (GEOBIA), for example, different soil (Dornik et al., 2018) or vegetation types (Kumar et al., 2019) or forest disturbances (Wang et al., 2019) can be mapped with high accuracy. Image time series allow the quantification of changes in land cover and land use over time (Cabral et al., 2018; Souza-Filho et al., 2016), including mineland revegetation (Nascimento et al., 2020). In addition, different vegetation indices, such as the normalized difference vegetation index (NDVI) (Jackson and Huete, 1991), allow the estimation of biomass accumulation (González-Alonso et al., 2006; Prabhakara et al., 2015), but the remote detection of further ecological attributes such as diversity, ecosystem functioning or environmental quality in rehabilitating minelands is still challenging (McKenna et al., 2020).

This challenge is because the environmental quality goes beyond the detection of land use changes or estimations about biomass accumulation and includes ecological functions ranging from trophic interactions to soil activity that operate at very different spatial scales (Mazón et al., 2019; James et al., 2020; Deng et al., 2020; Muñoz-Rojas, 2018). The recent statistical validation of tree diversity (out of a total of 27 individual, field-surveyed ecosystem properties) as the best indicator for the environmental quality of Amazonian minelands undergoing rehabilitation was an important milestone to simplify mineland monitoring (Gastauer et al., 2021). A procedure to detect tree diversity from high-resolution, multispectral satellite data (Torresani et al., 2019; Féret and Boissieu, 2020) may thus pave the way toward a remote sensing system for the environmental quality of minelands undergoing rehabilitation.

The spectral variation hypothesis is one of the main concepts used in recent decades to relate vegetation diversity to remotely sensed information (Gould, 2000; Palmer et al., 2002; Rocchini, 2007; Wang and Gamon, 2019): canopy characteristics, including leaf chemistry, orientation and distribution within the canopy, represent functional differences between species (Townsend et al., 2008; Reichstein et al., 2014) and result in differences in reflectance patterns measured from above (Clark et al., 2005; Féret and Asner, 2014). These spectral differences can be used to map certain species of interest, such as invasive species (Lehmann et al., 2017), when the pixel size is smaller than the canopies of focal plants (Turner, 2014). Based on the same logic, the degree of spectral variation among neighboring pixels may be used as a proxy for the diversity of vegetation (Chitale et al., 2019). To date, most research studies dealing with estimates of diversity derived from remote sensors have focused on mapping biodiversity hotspots (Rocchini et al., 2016). Nevertheless, procedures to detect tree diversity from multispectral satellite data (Torresani et al., 2019; Féret and Boissieu, 2020) may pave the way toward a remote sensing system for the environmental quality and successional advancement of minelands undergoing rehabilitation (Ganivet and Bloomberg, 2019; Chave et al., 2019). Using freely accessible satellite data during this monitoring may guarantee the transparency of mining companies' rehabilitation activities and their environmental commitment (Fuller, 2006).

The aim of this study was to develop a remote monitoring framework to assess the environmental quality of waste piles undergoing rehabilitation in the Carajás National Forest based on spectral diversity from freely available satellite images and open-source software. For this purpose, we categorized the field-surveyed rehabilitation status from a training data set (Gastauer et al., 2021) into five rehabilitation classes (Gann et al., 2019) and used these data to calibrate different indices of spectral diversity retrieved from Sentinel-2 images with the environmental quality of these areas. We optimized computation parameters (filtering options, user-defined number of clusters to categorize image pixels as spectral species, size of the plot buffer zones and selected spectral diversity metrics) of spectral diversity that maximized the accuracy of the remote monitoring approach, and we validated the procedure with an independent test data set. Based on selected parameters, we estimated the rehabilitating area and its quality based on five waste piles in the region and outlined environmental enhancements between 2017 and 2019.

2. Material and methods

2.1. Study site

This study was carried out using five mining waste piles from the N4-N5 iron mining complex and in the neighborhood of a small quarry called *Arenito* situated in the Carajás National Forest, Eastern Amazon, Pará, Brazil (Fig. 1). With a mean annual temperature of 26 °C, these sites have a tropical warm climate (Aw in the Köppen classification) with an annual precipitation of approximately 1,900 mm concentrated during rainy summers (Alvares et al., 2014). Vegetation is dominated by seasonal and evergreen dense submontane forests above deep oxisols, but iron rocks outcropping on mountain ridges are covered by ferruginous savanna formations, locally known as *cangas*. For iron mining, patchy *canga* vegetation, surrounding forests and large amounts of overburden are removed to reach the ore; the overburden is deposited in nearby sites forming large waste piles. To reduce the overall impact of mining activities on biodiversity and ecosystem services, waste piles are revegetated to trigger the launch of ecological succession toward natural ecosystems (forests). For this, waste pile benches are hydroseeded using native species from *canga* and forest ecosystems accompanied by commercial, fast-growing grasses and nitrogen-fixing legumes. Fertilization follows standardized recommendations (Guedes et al., 2021).

2.2. Rehabilitation status

For field-survey rehabilitation status, permanent plots of 10 × 20 m were installed in different rehabilitation stages (containing non-revegetated and rehabilitating benches of different ages as well as natural forest reference sites) within each waste pile for vegetation inventories and soil sampling, totaling 74 plots. Although up to 27 environmental variables were assessed in some of the plots (Gastauer et al., 2021), here, we used a reduced set of nine variables to estimate the rehabilitation status (Supplementary Material 1). This reduced set was available for a larger number of plots and was surveyed twice in some of the structures, enabling separation of a training data set (18 plots in WP NW2, 12 plots in WP West, 18 plots in WP S4 and 6 plots in Arenito, totaling 54 plots surveyed in 2017) and a testing data set (15 plots in WP NW2, 12 plots in WP West, 18 plots in WP S4, 9 plots in WP NW1 and 12 plots in WP N1, totaling 66 plots surveyed in 2019). The environmental variable set fulfills international monitoring standards, as variables related to (i) vegetation structure, (ii) community composition and diversity and (iii) ecological processes were also assessed (Gann et al., 2019). A previous study showed that a reduced variable set is sufficient to reliably describe actual rehabilitation status (for details, see Gastauer et al., 2021).

For the computation of rehabilitation status, the nine environmental variables were scaled, and a principal coordinate analysis (PCoA) was applied to address multicollinearity (Gastauer et al., 2020b). Then,

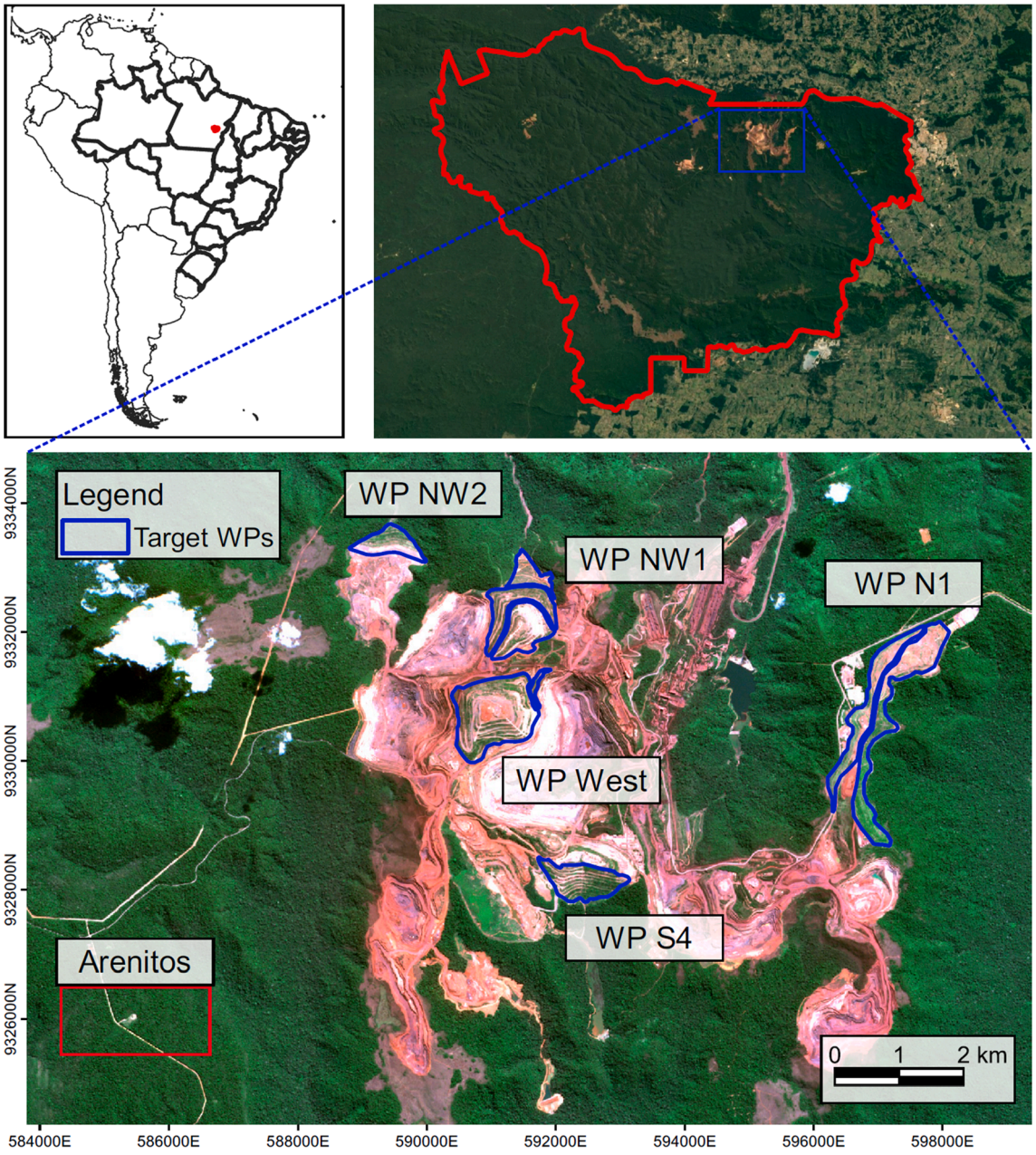

Fig. 1. Localization of target waste piles (WPs) in relation to the Carajás National Forest and South America. For WP NW1 and WP N1, only testing data are available; for *Arenito* reference plots, only training data are available.

rehabilitation status, i.e., the proportion of environmental advances still necessary to achieve predisturbance levels of the vegetation structure, community composition and diversity and ecological processes (in relation to the overall trajectory), was computed as follows:

$$Rehabilitation\ \ status = (1 - \frac{\Delta Reh - Ref}{\Delta NR - Ref}) * 100 \quad (1)$$

where ΔReh-Ref is the Euclidean distance between the plot's principal coordinates and the nearest reference plot and ΔNR-Ref is the nearest nonrevegetated-reference plot distance, i.e., the entire rehabilitation trajectory. Achieved scores followed Gann's et al.'s (2019) five-star approach. Plots with a rehabilitation status less than 2% received zero stars (i.e., nonrevegetated plots), and rehabilitation statuses reaching 20, 40, 60, 80 and 100% were classified as one-, two-, three-, four- and five-star rehabilitation, respectively, independent of stand age. Five-star rehabilitation was achieved by reference sites only.

2.3. Remote sensing data sources and preprocessing

We explored available images from the Sentinel-2 mission via the Copernicus Open Access Hub to identify cloud-free acquisitions above the target structures as close as possible to survey data, i.e., April 2017 for the training data set and April 2019 for the test data set. As atmospheric conditions during the rainy season (November-May) strongly reduce the availability of operable images, we used the search function from the Copernicus Open Access Hub to preselect for Sentinel-2 tiles T22MEU with less than 20% cloud cover between January and September 2017 (7 images) and 2019 (20 images). From that, we identified the images from June 30, 2017, and June 30, 2019, as those without cloud cover above the study area as close as possible to the field-surveyed data.

As Bottom-Of-Atmosphere (MSIL2A) versions of the images from 2017 are not available from the Copernicus Open Access Hub, we

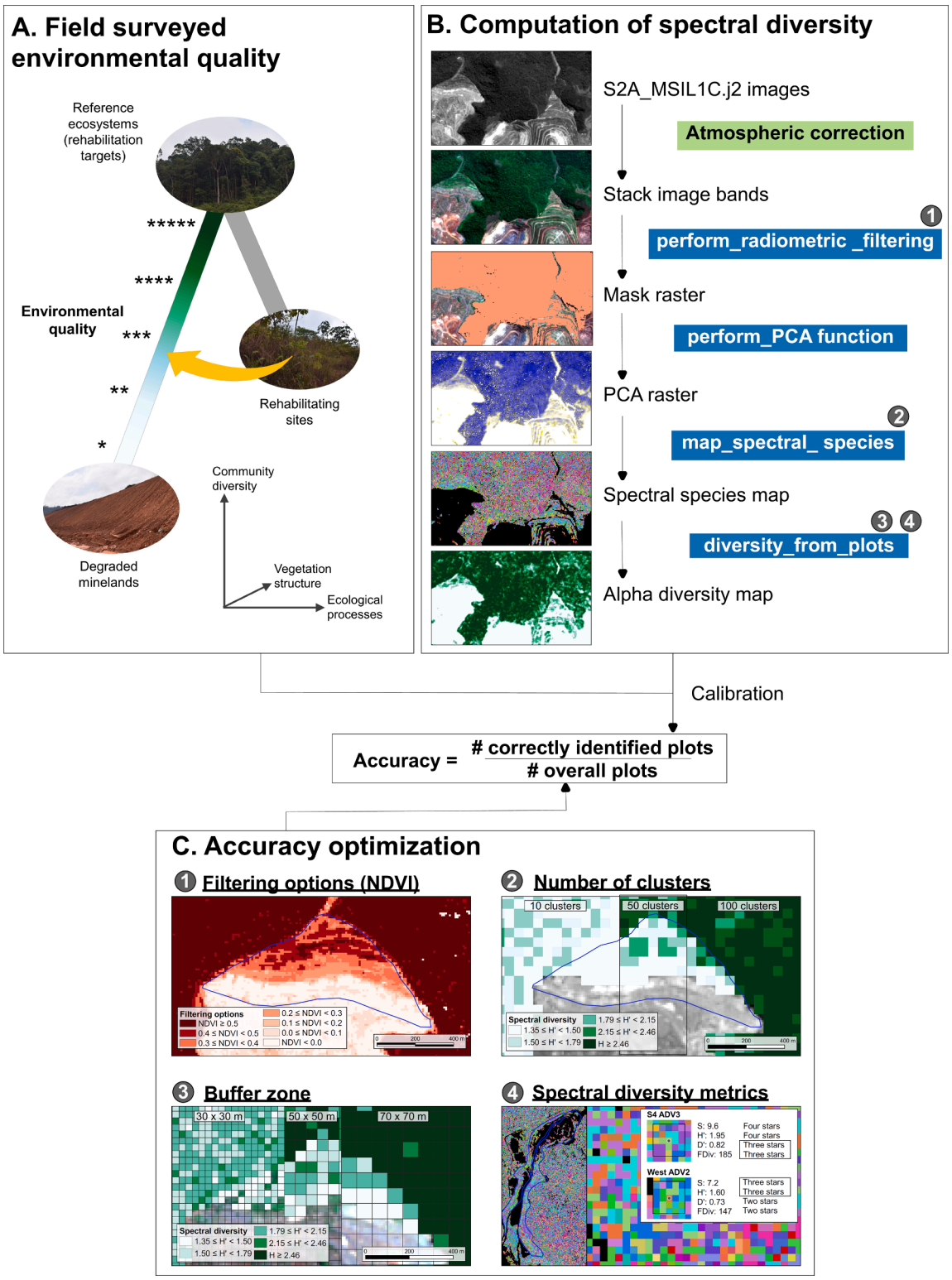

Fig. 2. Workflow for (A) the computation of environmental quality of rehabilitating minelands, (B) spectral alpha diversity from Sentinel-2A image sources and (C) accuracy optimization to enhance our remote sensing approach for mineland rehabilitation status. Atmospheric correction in (B) was carried out using the sen2cor algorithm in SNAP (ESA); blue fields refer to R commands from the biodivMapR package. Numbers in (B) refer to steps of parameter optimization in (C). Different colors in the spectral diversity map (Step 4 in C) refer to distinct spectral species; S is spectral species richness, H' is Shannon spectral diversity, D' is Simpson spectral diversity and FDiv is spectral functional divergence.

downloaded Top-Of-Atmosphere images (Levels-1A) and performed atmospheric corrections using the sen2cor tool from the Sentinel Application Platform (SNAP) toolbox (https://step.esa.int/main/toolboxes/snap/). After atmospheric correction, ten bands remained out of the thirteen original bands, and bands with 20 m spatial resolution were resampled to 10 m spatial resolution using the nearest neighbor algorithm. The resulting level 2A bands were then stacked and cropped to build the scene site shown in Fig. 1.

2.4. Spectral diversity

We analyzed spectral diversity from the Sentinel-2 images using the package biodivMapR (Féret and Boissieu, 2020) running in the R Environment (R Development Core Team, 2018). The method included in biodivMapR is an adaptation of the method initially developed by (Féret and Asner, 2014) to map α- and β-diversity from imaging spectroscopy acquired over tropical forests. This method requires image preparation, including multiple steps (Fig. 2B). The first step consists of masking irrelevant pixels. biodivMapR includes a set of basic radiometric filters aiming at discarding irrelevant pixels for the analysis: a thresholding applied on band B02 (blue) is applicable to eliminate potential haze or thin clouds characterized by higher reflectance than noncloudy vegetation; a thresholding applied on band B08 (near-infrared (NIR)) is applicable to eliminate shaded vegetation characterized by lower reflectance than sunlit vegetation. Finally, NDVI thresholding is applicable to mask nonvegetated pixels. NDVI values range from −1 to 1, with negative values generally attributed to water surfaces, while values of approximately 0 indicate bare soil, and positive values are associated with the density of vegetation cover (Tarpley et al., 1984).

In our study, the blue threshold was set to 10% reflectance, which is particularly high for vegetation, as our initial image selection guaranteed cloud- and haze-free pixels. Given the relevance of mixed pixels with a low vegetation fraction, we used a low NIR threshold (5%) to reduce the probability of masking mixed pixels. As rehabilitation chronosequences comprise different vegetation formations ranging from herbaceous communities to areas with a dense tree canopy, we tested different NDVI thresholds to separate nonvegetated from rehabilitating pixels to optimize the estimation of the rehabilitation status (optimization parameter 1 in Fig. 2B; see details below).

Once pixels for masking are identified, continuum removal is applied to reflectance data of the remaining pixels, followed by principal component analysis (PCA, Féret and Boissieu, 2020; Laliberté et al., 2020) and component selection based on visual interpretation. We used all principal components to proceed with the computation of spectral diversity. From that, a k-means clustering algorithm categorizes image pixels within a user-defined number of clusters, i.e., the total number of spectral species defined within the scene. From these spectral species maps, different measures of spectral diversity can be computed for each plot. Small field-surveyed plots (10 × 20 m) compared to Sentinel-2 resolution (10 × 10 m) impede the exact computation of per field-surveyed plot spectral diversity and require the definition of buffer zones. As plot orientation follows the terrain and varies between benches, we assumed quadratic buffer zones around the plot centroid, considering the field-surveyed diversity from the 10 × 20 m plot to be a sample of the entire diversity within the buffer zone.

2.5. Parameter optimization and accuracy assessment

To link remotely sensed spectral diversity to the field-surveyed rehabilitation status from the training data set, we defined boundary values able to classify spectral diversity within the six categories (zero to five-star rehabilitation) maximizing overall accuracy (Olofsson et al., 2014). Overall accuracy is here defined as the percentage of plots classified in the same categories by remotely sensed and field-surveyed data and was derived from confusion matrices (e.g., Fig. 2B). To maximize overall accuracy, we manually varied boundary values between categories in steps of 0.01. As in some cases more than one set of spectral diversity boundary values was able to maximize the overall accuracy, we selected the one that maximizes user and producer accuracy for the category within the five-star approach with the lowest performance.

The procedure used to identify the optimal parameterization of our analysis was performed as follows:

i. Definition of optimal NDVI threshold: NDVI threshold values ranging between 0 and 0.5 with 0.1 steps were applied to mask nonvegetated pixels (Step 1 in Fig. 2C). A buffer zone of 50 × 50 m around each plot centroid was defined, meaning that the Shannon index was computed from 25 pixels, and the number of clusters was set to 50 pixels in biodivMapR.
ii. Definition of the optimized size of the buffer zone around each plot: we compared the overall accuracy for buffer zones of 30 × 30 m, 50 × 50 m and 70 × 70 m around each plot centroid, which correspond to 3x3, 5x5 and 7x7 pixels in the Sentinel-2 image (Step 2 in Fig. 2C). The number of clusters was set to 50 pixels in biodivMapR, and the NDVI threshold was defined based on the optimal value identified in the previous step.
iii. Definition of the optimal number of clusters: We compared the overall accuracy for a number of clusters corresponding to 10, 20, 50, 100, 150 and 200 spectral species to be identified from the selection of components of the PCA (Step 3 in Fig. 2C). The NDVI threshold and buffer size were defined based on the optimal values identified in the previous steps.
iv. Finally, multiple spectral diversity indices, including (i) species richness (S), (ii) Shannon's index (H'), (iii) Simpson (D') and (iv) functional divergence (FDiv), were computed from each plot using the optimal parameterization described previously, and their capacity to discriminate among rehabilitation statuses was compared based on overall accuracy, following the same procedure (Step 4 in Fig. 2C).

2.6. Environmental enhancements at the study sites between 2017 and 2019

Using optimized computation parameters, we computed spectral diversity for the testing data set. Based on boundary values between rehabilitation categories maximizing the overall accuracy in the training data set, we classified spectral diversity from the testing data set within the six categories from the five-star approach and detected the overall accuracy.

Then, we used optimized computational parameters to compute a spectral diversity raster. For that, we built virtual plots so that each pixel centroid coordinate from the satellite image became the centroid of a virtual plot. For each pixel, we computed the spectral diversity from both images (2017 and 2019). We classified spectral diversity in the six rehabilitation categories (zero- to five-star rehabilitation) using boundary values from the previous section. For both years, we counted the number of pixels from each category within the five monitored structures (delimited by blue lines in Fig. 1) using the extract function from the 'raster' package in the R Environment (Hijmans and van Etten, 2020). Based on the number of pixels from each category and confusion matrix, we estimated the area in each category and 95% confidence intervals as suggested by Olofsson et al. (2014).

3. Results

3.1. Optimization of computation parameters

Spectral diversity computed for the training data set was positively associated with field-detected environmental quality, but the accuracy of the remote recognition of rehabilitation status differed among optimization runs (Fig. 3). The value of the NDVI thresholds strongly influenced the number of pixels selected for the computation of spectral diversity, and the highest overall accuracy was achieved using an NDVI of 0.2. During this computation, eight out of ten nonrevegetated bare soil plots were recognized as such, and only one rehabilitating plot (out of 44 from the training data set) was masked for subsequent analysis. Larger NDVI thresholds did not target some of the rehabilitation plots, as 3, 15, and 26 rehabilitation plots were masked when using NDVI values of 0.3, 0.4 and 0.5, respectively. Furthermore, smaller NDVI values maintained plots without vegetation within the analysis, reducing the correlation coefficients between spectral diversity and field-detected

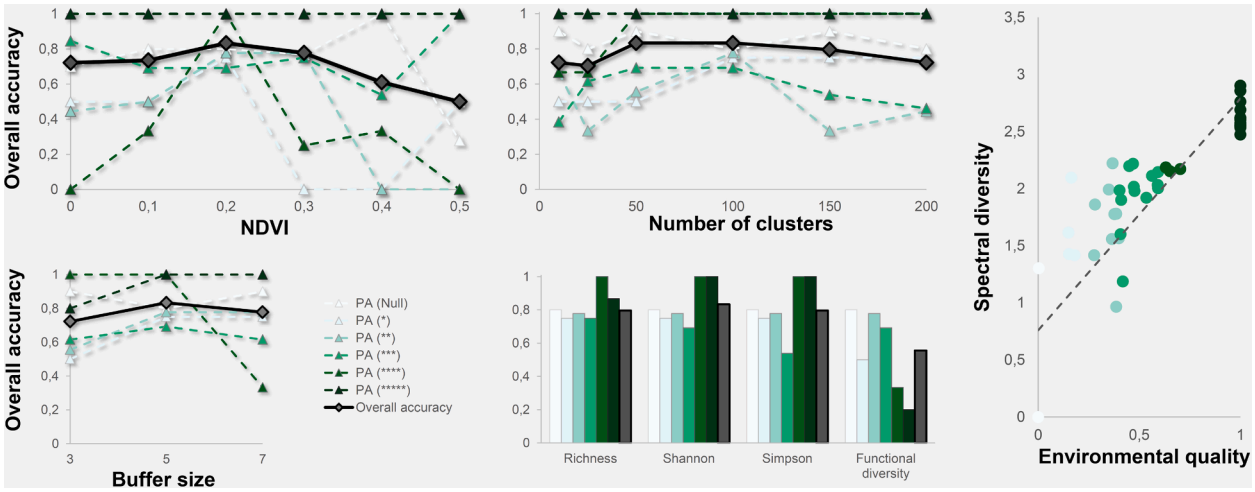

Fig. 3. Influence of the NDVI (A), number of clusters (B), size of the buffer zone (C) and the spectral diversity metric (D) on the overall and producer accuracy (PA) retrieved from satellite images matching the field-surveyed rehabilitation status for the training data set and correlation between field-surveyed environmental quality and remotely detected spectral diversity (E).

rehabilitation status as well as overall accuracy for remotely detecting the rehabilitation status. Detailed information on overall, producer and user accuracy is provided in Supplementary Materials 2 and 3.

The overall accuracy was highest when using the intermediate buffer zone (50 × 50 m). The smaller buffer zone (30 × 30 m) tended to underestimate the spectral diversity in the reference plots. Some plots did not receive diversity values when buffer zones comprising 70 × 70 m were used, reducing overall accuracy (Supplementary Materials 2 and 3). The overall accuracy was highest when the PCA output was clustered in 50 and 100 clusters (Fig. 3), but the producer accuracy of single categories was better when 100 clusters were used for computation. Finally, the Shannon index of spectral diversity performed slightly better

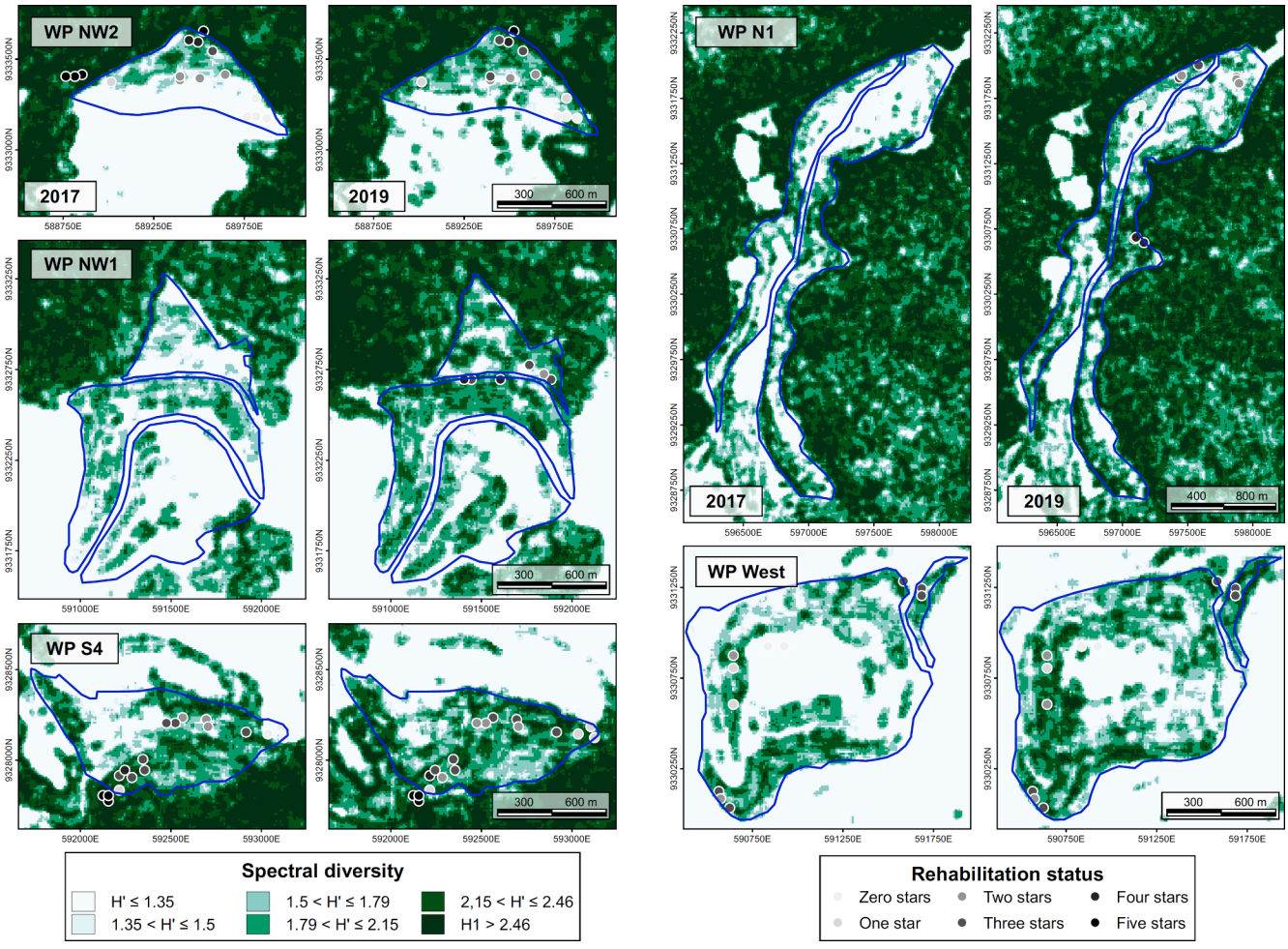

Fig. 4. Shannon spectral diversity retrieved from the Sentinel-2A satellite image from June 30th, 2017, and June 30th, 2019, for the five monitored waste piles.

than the Simpson diversity or spectral species richness, and the lowest overall accuracy was achieved by functional spectral diversity, which does not rely on clustering of PCA outputs (Fig. 3).

Based on the highest overall accuracy (83%), we proceeded with the Shannon index of spectral diversity computed using an NDVI of 0.2, a cluster number of 100 and a buffer zone of 50 × 50 m to compute spectral diversity for 2017 (Fig. 4). The standard deviation of principal components was reduced from 1.992 for principal component 1 (PC1), explaining 0.496 of the variance, to 0.1777 for PC8, with 0.004% of the total variance explained (Supplementary Material 4). The boundary values of the Shannon spectral diversity between the rehabilitation categories were 1.35 (zero to one star), 1.5 (one to two stars), 1.79 (two to three stars), 2.15 (three to four stars) and 2.46 (four to five stars). The producer accuracies varied between 0.692 for three-star rehabilitation and 1.000 for four- and five-star rehabilitation, and user accuracy ranged between 0.600 for four-star rehabilitation and 1.000 for one- and five-star rehabilitation (Fig. 3; Supplementary Material 2 and 3).

3.2. Changes in the rehabilitation status between 2017 and 2019

The resampling of field and remote sensing data in 2019 (testing data set) using the same boundary values found for the training data set produced an overall accuracy of 0.833, but the producer and user accuracies showed some differences compared to the training data set (Table 1). User accuracy increased for zero-, three- and four-star rehabilitation. The producer accuracy increased for two- and three-star rehabilitation but decreased for zero- and one-star rehabilitation (Table 1).

Within the target structures, gains and losses of spectral diversity occurred between 2017 and 2019, indicating changes in the environmental quality of the monitored waste piles (Fig. 5). Rehabilitation areas with elevated spectral diversity in 2017, e.g., the northern part of WP NW2 or northwest of WP West, fluctuated slightly, showing small gains or losses, similar to what seems to correspond to the natural dynamics of mature forests adjacent to the mines. Punctual deteriorations of spectral diversity were detected all over WP NW1, in the central part of WP N1 and the eastern part of WP West. More comprehensive losses of spectral diversity were found in the southeastern part of WP NW1 (number 2 in Fig. 5), the southern part of WP West (3), the southeastern portion of WP S4 (4) and the central part of WP N1 (7). Additional significant losses outside target structures resulted from the removal of temporary revegetation as a function of ongoing mining activities, e.g., continuous filling of WP S4 on its top section (5), the construction of a draining system at the base of WP S4 (6) or vegetation logging as mining activities advance (east to WP NW1, 1).

Comprehensive enhancements in spectral diversity occurred in the upper part of WP NW2, entire WP NW1, WP West, western part of WP S4 and northeastern WP N1. Due to these enhancements, the overall rehabilitation area increased between 2017 and 2019 from 275.79 to 366.82 ha within all five monitored waste piles (Fig. 6). The area of one-star rehabilitation remained unchanged, but the amount of two-, three-, four- and five-star rehabilitation increased by 9.03 ha (9.68%), 35.30 ha (25.34%), 34.63 ha (42.25%), and 13.10 ha (65.33%), respectively (Table 2).

4. Discussion

Our findings show that the spectral diversity computed from publicly available Sentinel-2 imagery is positively associated with measures of environmental quality that integrate above- and belowground measures regarding community diversity, vegetation structure and ecological processes in waste pile benches from the N4-N5 mining complex in the Carajás National Forest. Previous studies identified tree diversity as a powerful surrogate for the overall environmental quality of minelands undergoing rehabilitation (Gastauer et al. 2021), so our findings are consistent with the spectral diversity hypothesis (Jetz et al., 2016). After optimization of computation parameters to maximize forecast accuracy using high-quality ground data for calibration, these results open perspectives for the remote monitoring of the environmental quality of rehabilitation activities. The automatization of mineland rehabilitation monitoring systems based on freely available satellite images and open-source software enables the upscaling and cost reduction of monitoring activities. Such applications would furthermore answer the need for independent verification of enhancements or degradation of rehabilitation areas, making the rehabilitation activities of mining companies transparent by remote quality assessments.

The highest accuracy values between remote and field-surveyed rehabilitation status were detected when the Shannon spectral diversity was computed using an NDVI threshold of 0.2, buffer zones of 50x50 m and 100 clusters. The NDVI threshold of 0.2 adequately separated nonvegetated pixels from pixels, indicating rehabilitation within the available images. However, short-term water availability, seasonality, management and other factors influence the vigor of vegetation and thus NDVI (Gurgel and Ferreira, 2003; Liu et al., 2013), so the NDVI threshold used here may not apply to images from further seasons. Although larger buffer zones should more accurately describe diversity patterns (Crawley and Harral, 2001), buffer zones were limited by the width of the waste pile benches, and 50 × 50 m performed best.

Accuracy increased up to 100 clusters, but more than 100 clusters disproportionally increased the spectral diversity of rehabilitation plots, reducing user and producer accuracies in the lower rehabilitation categories. The usage of 100 clusters seems plausible because 197 species were sampled during field surveys, including many understory species invisible from the upper canopy. Shannon diversity performed better than spectral species richness and Simpson diversity, confirming previous studies (Oldeland et al., 2010). Functional diversity considered spectral differences among plots within the buffer zone and performed less accurately for the detection of rehabilitation status. Assuming that spectral differences are related to functional differences among plants/trees from different pixels, this is consistent with field-surveyed data, where functional tree diversity was a poor predictor of environmental quality in rehabilitation areas, as functional diversity recovered rapidly (Gastauer et al., 2021).

High accuracy for both training and testing data sets encourages the

Table 1
Confusion matrix, overall, producer and user accuracies for Shannon spectral diversity to classify the rehabilitation status of the testing data set.

		Field-measured rehabilitation status							
		Null	*	**	***	****	*****	**Sum**	**User accuracy**
Remotely detected rehabilitation status	**Null**	**10**	0	1	0	0	0	**11**	**0.909**
	*	0	**3**	0	0	0	0	**3**	**1.000**
	**	2	1	**12**	1	0	0	**16**	**0.750**
	***	0	2	1	**18**	0	0	**21**	**0.857**
	****	0	1	1	1	**6**	0	**9**	**0.667**
	*****	0	0	0	0	0	**6**	**6**	**1.000**
	Sum	**12**	**7**	**15**	**20**	**6**	**6**	**66**	
	Producer accuracy	**0.833**	**0.429**	**0.800**	**0.900**	**1.000**	**1.000**		
Overall accuracy									**0.833**

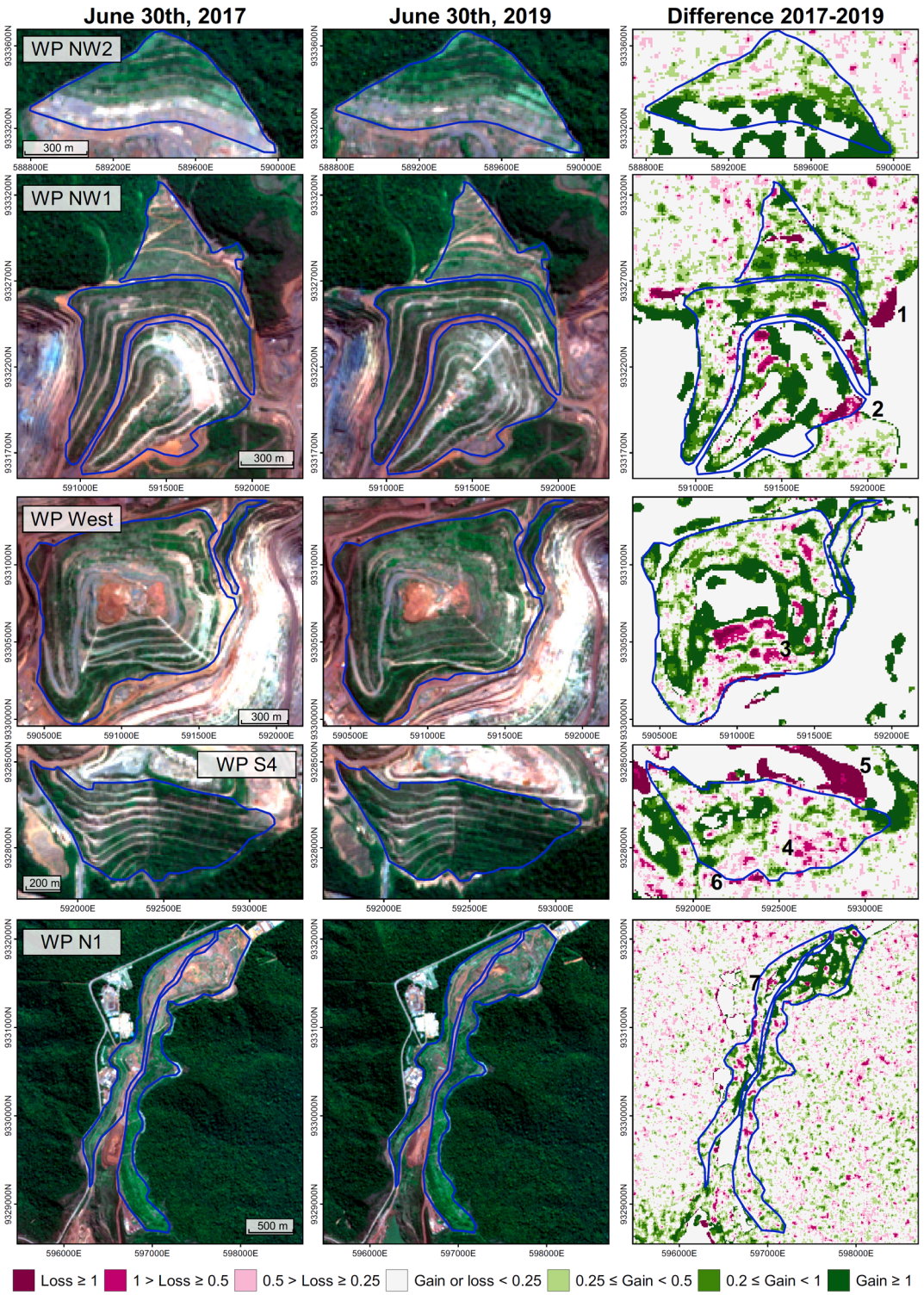

Fig. 5. Sentinel-2 images from 2017 and 2019 and changes in the spectral diversity of five waste piles undergoing rehabilitation from the N4-N5 mining complex in the Carajás National Forest between 2017 (training data set) and 2019 (testing data set). For correct localization of the target structures, please refer to Fig. 1. For the meaning of embedded numbers in maps of spectral diversity changes, please refer to the main text.

inclusion of the presented approach within existing mineland monitoring protocols. In doing so, punctual losses and comprehensive gains of spectral diversity were detected between 2017 and 2019. Some of the losses of spectral diversity identified here result from the removal of temporary rehabilitation or spontaneous vegetation due to infrastructure projects or ongoing waste pile filling. Further losses appear in disturbed sites, e.g., after landslides. In contrast, comprehensive gains in spectral diversity result from increasing amounts of revegetated and rehabilitation areas as well as from gains in spectral diversity of already revegetated areas. Net gains in the absolute amount of rehabilitation areas result from active rehabilitation or spontaneous vegetation establishment, which is in line with previous findings (Nascimento et al., 2020). However, increases in the spectral diversity of already revegetated areas indicate enhancements in the rehabilitation status and are

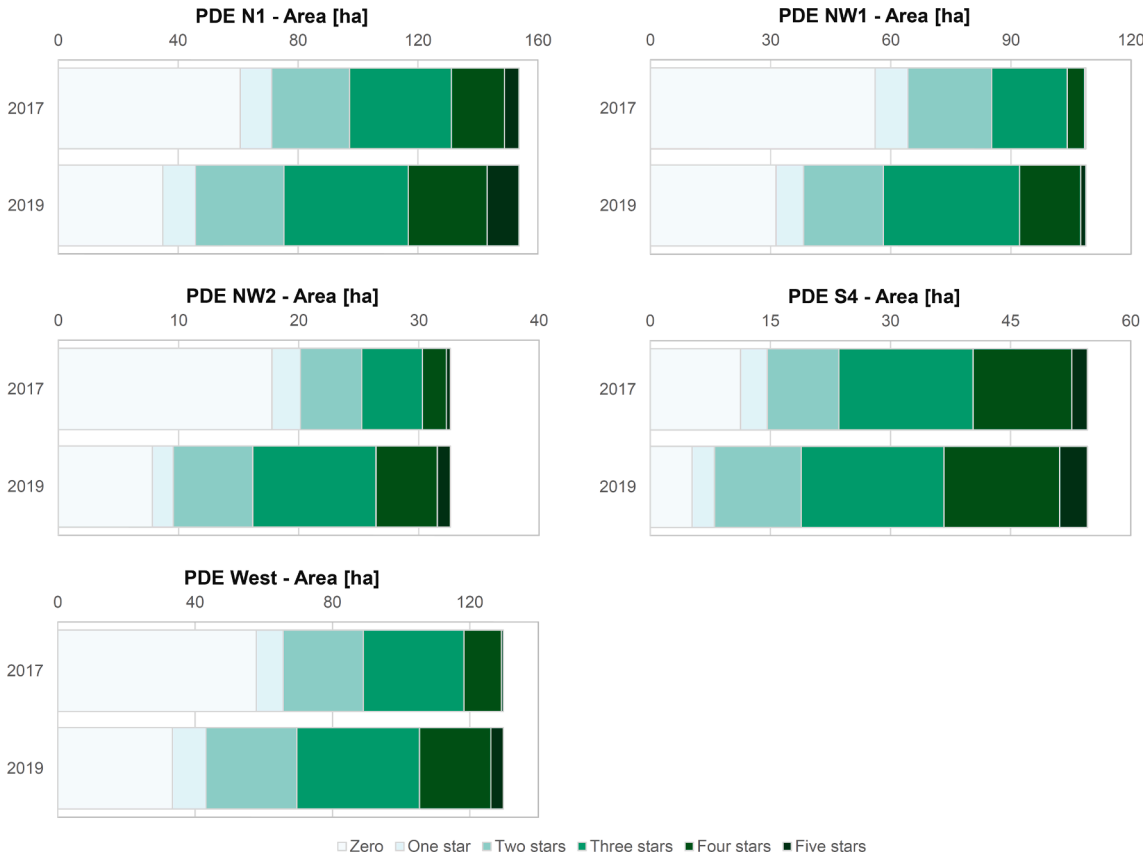

Fig. 6. Remotely detected changes in the amount and environmental quality of rehabilitation between 2017 and 2019 for five waste piles in the Carajás National Forest, Eastern Amazon, Brazil. Net gains in the rehabilitation areas result from rehabilitation activities or spontaneous vegetation establishment, while enhancements in already revegetated areas indicate the successional advancement of these areas with time.

Table 2
Changes in the area of rehabilitation between 2017 and 2019 (including 95% confidence intervals) for five waste piles in the Carajás National Forest, Eastern Amazon, Brazil.

Rehabilitation category	2017 [ha ± 95% CI]	2019 [ha ± 95% CI]	Difference [ha]	Difference [%]
Null	203.67 ± 49.34	112.61 ± 25.65	−91.06	−80.86
*	32.20 ± 24.31	32.19 ± 27.59	−0.01	−0.03
**	84.25 ± 54.14	93.28 ± 36.11	9.03	9.68
***	104.02 ± 40.85	139.32 ± 30.06	35.30	25.34
****	47.32 ± 23.03	81.96 ± 25.58	34.63	42.25
*****	7.95 ± 0.00	20.05 ± 0.00	13.10	65.33

consistent with successional advances in tree diversity and rehabilitation status over time (Gastauer et al., 2019). If validated by further ground data, these comprehensive gains of spectral diversity will contribute to demonstrating how rehabilitation activities reduce the overall environmental impact of mining operations.

The empirical approach for parameter optimization to compute spectral diversity that best tracks the environmental status of minelands undergoing rehabilitation was straightforward, but some points require further investigation. First, computational parameter optimization may require further enhancements, as the relationship between NDVI, seasonality, interannual climatic variation and spectral diversity remains unclear. Threshold values between rehabilitation categories may require further calibration when remote sensing images with other timestamps from different seasons or different spectral bands are applied to compute spectral diversity. Second, the spatial, temporal and spectral resolutions of diversity maps produced here are limited by the availability of adequate satellite images. High-resolution commercial satellites or year-round images of high spatial and spectral resolution provided by remotely piloted aircraft systems may enable and enhance (i) the remote sensing of the environmental status in rehabilitation areas smaller than those observed here (e.g., narrow benches of cut slopes from mine pits, Nascimento et al., 2020), (ii) the real-time detection of declines in species diversity and environmental quality to support the management of these areas, and by using the concept of spectral species, (iii) the mapping of single tree species that require attention, such as alien invaders. Finally, more ground data than actually available from the N4-N5 mining complex and further rehabilitation projects are necessary to validate the detected changes in spectral diversity and generalize our findings. However, accuracies higher than 80% in both training and testing data to remotely detect environmental quality representing the key ecological attributes motivate the integration of the presented approach in existing mineland monitoring protocols.

5. Conclusion

Although a set of issues needs to be investigated to advance and enhance the presented framework, the high accuracy of the presented remote monitoring scheme encourages the application of spectral diversity retrieved from high-resolution satellite images to identify environmental gains and losses in minelands from the Carajás National Forest undergoing rehabilitation. The application simplifies the overall monitoring procedure by reducing costs and operational risks and

credits large-scale rehabilitation activities carried out to reduce the environmental impact of mining activities, and the automated identification of eventual degradations by losses in spectral diversity permits timely remedial measures where necessary. The usage of free software and free satellite imagery, although limited by the spatial and/or spectral resolution of the available images, enables furthermore the independent verification of annual reports by licensing agencies, thus making a company's environmental commitment to rehabilitation activities transparent. Thus, the calibration of spectral diversity to detect the environmental quality of rehabilitating sites from further regions may open new avenues for the large-scale monitoring of minelands undergoing rehabilitation.

Declaration of Competing Interest

The authors declare that they have no known competing financial interests or personal relationships that could have appeared to influence the work reported in this paper.

Acknowledgments

This work was funded by Instituto Tecnológico Vale (RAD I) and received additional support by CNPq to SJR (305831/2016-0) and PWMSF (306430/2013-5). JBF acknowledges financial support from Agence Nationale de la Recherche (France) (BioCop project—ANR-17-CE32-0001). We are grateful for valuable comments from two anonymous reviewers.

Appendix A. Supplementary material

Supplementary data to this article can be found online at https://doi.org/10.1016/j.jag.2021.102653.

References

de Almeida, D.R.A., Stark, S.C., Valbuena, R., Broadbent, E.N., Silva, T.S.F., de Resende, A.F., Ferreira, M.P., Cardil, A., Silva, C.A., Amazonas, N., Zambrano, A.M. A., Brancalion, P.H.S., 2020. A New Era in Forest Restoration Monitoring. Restor. Ecol. 28 (1), 8–11.

Alvares, C.A., Stape, J.L., Sentelhas, P.C., de Moraes Gonçalves, J.L., Sparovek, G., 2014. Köppen's Climate Classification Map for Brazil. Meteorol. Z. 22 (6), 711–728.

Cabral, A.I.R., Saito, C., Pereira, H., Laques, A.E., 2018. Deforestation pattern dynamics in protected areas of the Brazilian Legal Amazon using remote sensing data. Appl. Geogr. 100, 101–115.

Chave, J., Davies, S.J., Phillips, O.L., Lewis, S.L., Sist, P., Schepaschenko, D., Armston, J., Baker, T.R., Coomes, D., Disney, M., Duncanson, L., Hérault, B., Labrière, N., Meyer, V., Réjou-Méchain, M., Scipal, K., Saatchi, S., 2019. Ground Data Are Essential for Biomass Remote Sensing Missions. Surv. Geophys. 40 (4), 863–880.

Chitale, V.S., Behera, M.D., Roy, P.S., 2019. Deciphering Plant Richness Using Satellite Remote Sensing: A Study from Three Biodiversity Hotspots. Biodivers. Conserv. 28 (8-9), 2183–2196.

Clark, M., Roberts, D., Clark, D., 2005. Hyperspectral Discrimination of Tropical Rain Forest Tree Species at Leaf to Crown Scales. Remote Sens. Environ. 96 (3-4), 375–398.

Crawley, M.J., Harral, J.E., 2001. Scale Dependence in Plant Biodiversity. Science 291 (5505), 864–868.

Deng, J., Bai, X., Zhou, Y., Zhu, W., Yin, Y., 2020. Variations of Soil Microbial Communities Accompanied by Different Vegetation Restoration in an Open-Cut Iron Mining Area. The Science of the Total Environment 704, 135243. https://doi.org/10.1016/j.scitotenv.2019.135243.

Dornik, A., Drăguţ, L., Urdea, P., 2018. Classification of Soil Types Using Geographic Object-Based Image Analysis and Random Forests. Pedosphere 28 (6), 913–925.

Féret, J.-B., Asner, G.P., 2014. Mapping Tropical Forest Canopy Diversity Using High-Fidelity Imaging Spectroscopy. Ecological Applications: A Publication of the Ecological Society of America 24 (6), 1289–1296.

Féret, J.-B., Boissieu, F., 2020. "biodivMapR: An R Package for α- and β-diversity Mapping Using Remotely Sensed Images". Edited by Kylie Scales. Methods in Ecology and Evolution / British Ecological Society 11 (1), 64–70.

Fuller, D.O., 2006. Tropical Forest Monitoring and Remote Sensing: A New Era of Transparency in Forest Governance? Singap. J. Trop. Geogr. 27 (1), 15–29.

Ganivet, E., Bloomberg, M., 2019. Towards Rapid Assessments of Tree Species Diversity and Structure in Fragmented Tropical Forests: A Review of Perspectives Offered by Remotely-Sensed and Field-Based Data. For. Ecol. Manage. 432 (January), 40–53.

Gann, G.D., McDonald, T., Walder, B., Aronson, J., Nelson, C.R., Jonson, J., Hallett, J.G., Eisenberg, C., Guariguata, M.R., Liu, J., Hua, F., Echeverría, C., Gonzales, E., Shaw, N., Decleer, K., Dixon, K.W., 2019. International Principles and Standards for the Practice of Ecological Restoration. Second Edition. Restor. Ecol. 27 (S1) https://doi.org/10.1111/rec.v27.S110.1111/rec.13035.

Gastauer, M., Caldeira, C.F., Ramos, S.J., Silva, D.F., Siqueira, J.O., 2020a. Active Rehabilitation of Amazonian Sand Mines Converges Soils, Plant Communities and Environmental Status to Their Predisturbance Levels. *Land Degrad. Dev.*, October. 31 (5), 607–618. https://doi.org/10.1002/ldr.3475.

Gastauer, M., Caldeira, C.F., Ramos, S.J., Trevelin, L.C., Jaffé, R., Oliveira, G., Vera, M.P. O., Pires, E., Santiago, F.L.d.A., Carneiro, M.A.C., Coelho, F.T.A., Silva, R., Souza-Filho, P.W.M., Siqueira, J.-O., 2020b. Integrating Environmental Variables by Multivariate Ordination Enables the Reliable Estimation of Mineland Rehabilitation Status. J. Environ. Manage. 256, 109894. https://doi.org/10.1016/j.jenvman.2019.109894.

Gastauer, M., Sarmento, P.S.d.M., Caldeira, C.F., Castro, A.F., Ramos, S.J., Trevelin, L.C., Jaffé, R., Rosa, G.A., Carneiro, M.A.C., Valadares, R.B.d.S., Oliveira, G., Souza Filho, P.W.M., 2021. Shannon Tree Diversity Is a Surrogate for Mineland Rehabilitation Status. Ecol. Ind. 130, 108100. https://doi.org/10.1016/j.ecolind.2021.108100.

Gastauer, M., Silva, J.R., Junior, C.F.C., Ramos, S.J., Filho, P.W.M.S., Neto, A.E.F., Siqueira, J.O., 2018. Mine Land Rehabilitation: Modern Ecological Approaches for More Sustainable Mining. J. Cleaner Prod. 172 (January), 1409–1422.

Gastauer, M., Souza Filho, P.W.M., Ramos, S.J., Caldeira, C.F., Silva, J.R., Siqueira, J.O., Furtini Neto, A.E., 2019. Mine Land Rehabilitation in Brazil: Goals and Techniques in the Context of Legal Requirements. *Ambio*, April. 48 (1), 74–88. https://doi.org/10.1007/s13280-018-1053-8.

González-Alonso, F., Merino-De-Miguel, S., Roldán-Zamarrón, A., García-Gigorro, S., Cuevas, J.M., 2006. Forest Biomass Estimation through NDVI Composites. The Role of Remotely Sensed Data to Assess Spanish Forests as Carbon Sinks. Int. J. Remote Sens. 27 (24), 5409–5415.

Gould, W., 2000. Remote Sensing of Vegetation, Plant Species Richness, and Regional Biodiversity Hotspots. Ecological Applications: A Publication of the Ecological Society of America 10 (6), 1861–1870.

Guedes, Rafael Silva, Sílvio Junio Ramos, Markus Gastauer, Cecílio Frois Caldeira Júnior, Gabriel Caixeta Martins, Wilson da Rocha Nascimento Júnior, Pedro Walfir Martins de Souza-Filho, and José Oswaldo Siqueira. 2021. "Challenges and Potential Approaches for Soil Recovery in Iron Open Pit Mines and Waste Piles." *Environmental Earth Sciences* 80 (18): 640.

Guerra, A., Reis, L.K., Borges, F.L.G., Ojeda, P.T.A., Pineda, D.A.M., Miranda, C.O., Maidana, D.P.F.d.L., Santos, T.M.R.D., Shibuya, P.S., Marques, M.C.M., Laurance, S. G.W., Garcia, L.C., 2020. Ecological Restoration in Brazilian Biomes: Identifying Advances and Gaps. For. Ecol. Manage. 458, 117802. https://doi.org/10.1016/j.foreco.2019.117802.

Gurgel, H.C., Ferreira, N.J., 2003. Annual and Interannual Variability of NDVI in Brazil and Its Connections with Climate. Int. J. Remote Sens. 24 (18), 3595–3609.

Hijmans, R.J., van Etten, J., 2020. Raster: Geographic Data Analysis and Modeling. R Package Version 2 (8).

Jackson, R.D., Huete, A.R., 1991. Interpreting Vegetation Indices. Preventive Veterinary Medicine 11 (3-4), 185–200.

James, W.R., Lesser, J.S., Litvin, S.Y., Nelson, J.A., 2020. Assessment of Food Web Recovery Following Restoration Using Resource Niche Metrics. The Science of the Total Environment 711, 134801. https://doi.org/10.1016/j.scitotenv.2019.134801.

Jetz, W., Cavender-Bares, J., Pavlick, R., Schimel, D., Davis, F.W., et al., 2016. JMonitoring plant functional diversity from space. Nat. Plants 2, 16024.

Johansen, K., Erskine, P.D., McCabe, M.F., 2019. Using Unmanned Aerial Vehicles to Assess the Rehabilitation Performance of Open Cut Coal Mines. J. Cleaner Prod. 209 (February), 819–833.

Kerr, J.T., Ostrovsky, M., 2003. From Space to Species: Ecological Applications for Remote Sensing. Trends Ecol. Evol. 18 (6), 299–305.

Kumar, S.S., Hanan, N.P., Prihodko, L., Julius Anchang, C., Ross, W., Ji, W., Lind, B.M., 2019. Alternative Vegetation States in Tropical Forests and Savannas: The Search for Consistent Signals in Diverse Remote Sensing Data. Remote Sensing 11 (7), 815.

Laliberté, E., Schweiger, A.K., Legendre, P., He, F., 2020. Partitioning plant spectral diversity into alpha and beta components. Ecol. Lett. 23 (2), 370–380.

Lamb, D., Erskine, P.D., Fletcher, A., 2015. Widening Gap between Expectations and Practice in Australian Minesite Rehabilitation. Ecol. Manage. Restor. 16 (3), 186–195.

Latawiec, A., Agol, D., 2016. *Sustainability Indicators in Practice*. De Gruyter Open, Poland, Warsaw, p. 271p.

Lechner, A.M., Foody, G.M., Boyd, D.S., 2020. Applications in Remote Sensing to Forest Ecology and Management. One Earth 2 (5), 405–412.

Lechner, A. M., S. Arnold, N. B. McCaffrey, A. Gordon, P. D. Erskine, M. J. Gillespie, and D. R. Mulligan. 2018. "Applying Modern Ecological Methods for Monitoring and Modelling Mine Rehabilitation Success." *From Start to Finish – a Life-of-Mine Perspective*, no. January: 109–16.

Lehmann, J.R.K., Prinz, T., Ziller, S.R., Thiele, J., Heringer, G., Meira-Neto, J.A.A., Buttschardt, T.K., 2017. Open-Source Processing and Analysis of Aerial Imagery Acquired with a Low-Cost Unmanned Aerial System to Support Invasive Plant Management. Front. Environ. Sci. Eng. China 5, 44.

Liu, G., Liu, H., Yin, Y.i., 2013. Global Patterns of NDVI-Indicated Vegetation Extremes and Their Sensitivity to Climate Extremes. Environmental Research Letters: ERL [Web Site] 8 (2), 025009. https://doi.org/10.1088/1748-9326/8/2/025009.

Martin, Roberta E. 2020. "Lessons Learned from Spectranomics: Wet Tropical Forests." In *Remote Sensing of Plant Biodiversity*, edited by Jeannine Cavender-Bares, John A. Gamon, and Philip A. Townsend, 105–20. Cham: Springer International Publishing.

Mazón, M., Aguirre, N., Echeverría, C., Aronson, J., 2019. Monitoring Attributes for Ecological Restoration in Latin America and the Caribbean Region. Restor. Ecol. 27 (5), 992–999.
McKenna, P.B., Lechner, A.M., Phinn, S., Erskine, P.D., 2020. Remote Sensing of Mine Site Rehabilitation for Ecological Outcomes. A Global Systematic Review. Remote Sensing 12 (21), 3535. https://doi.org/10.3390/rs12213535.
Muñoz-Rojas, M., 2018. Soil Quality Indicators: Critical Tools in Ecosystem Restoration. Current Opinion in Environmental Science & Health 5 (October), 47–52.
Nascimento, F.S., Gastauer, M., Pedro, W.M., Souza-Filho, W.R., Jr, N., Santos, D.C., Costa, M.F., 2020. Land Cover Changes in Open-Cast Mining Complexes Based on High-Resolution Remote Sensing Data. Remote Sensing 12 (4). https://doi.org/10.3390/rs12040611.
Oldeland, J., Dorigo, W., Lieckfeld, L., Lucieer, A., Jürgens, N., 2010. Combining Vegetation Indices, Constrained Ordination and Fuzzy Classification for Mapping Semi-Natural Vegetation Units from Hyperspectral Imagery. Remote Sens. Environ. 114 (6), 1155–1166.
Olofsson, P., Foody, G.M., Herold, M., Stehman, S.V., Woodcock, C.E., Wulder, M.A., 2014. Good Practices for Estimating Area and Assessing Accuracy of Land Change. Remote Sens. Environ. 148 (May), 42–57.
Palmer, M.W., Earls, P.G., Hoagland, B.W., White, P.S., Wohlgemuth, T., 2002. Quantitative Tools for Perfecting Species Lists. Environmetrics 13 (2), 121–137.
Perring, M.P., Standish, R.J., Price, J.N., Craig, M.D., Erickson, T.E., Ruthrof, K.X., Whiteley, A.S., Valentine, L.E., Hobbs, R.J., 2015. Advances in Restoration Ecology: Rising to the Challenges of the Coming Decades. Ecosphere 6 (8), art131. https://doi.org/10.1890/ES15-00121.1.
Prabhakara, K., Dean Hively, W., McCarty, G.W., 2015. Evaluating the Relationship between Biomass, Percent Groundcover and Remote Sensing Indices across Six Winter Cover Crop Fields in Maryland, United States. Int. J. Appl. Earth Obs. Geoinf. 39 (July), 88–102.
R Development Core Team. 2018. "R: A Language and Environment for Statistical Computing, R Foundation for Statistical Computing." Vienna.
Reichstein, M., Bahn, M., Mahecha, M.D., Kattge, J., Baldocchi, D.D., 2014. Linking Plant and Ecosystem Functional Biogeography. PNAS 111 (38), 13697–13702.
Rocchini, D., 2007. Effects of Spatial and Spectral Resolution in Estimating Ecosystem α-Diversity by Satellite Imagery. Remote Sens. Environ. 111 (4), 423–434.
Rocchini, D., Boyd, D.S., Féret, J.-B., Foody, G.M., He, K.S., Lausch, A., Nagendra, H., Wegmann, M., Pettorelli, N., Skidmore, A., Chauvenet, A., 2016. Satellite remote sensing to monitor species diversity: potential and pitfalls. Remote Sens Ecol Conserv 2 (1), 25–36.
Ruiz-Jaén, M.C., Aide, T.M., 2005. Vegetation structure, species diversity, and ecosystem processes as measures of restoration success. For. Ecol. Manage. 218 (1-3), 159–173. https://doi.org/10.1016/j.foreco.2005.07.008.
Sonter, L.J., Dade, M.C., Watson, J.E.M., Valenta, R.K., 2020. Renewable energy production will exacerbate mining threats to biodiversity. Nat. Commun. 11 (1), 4174. https://doi.org/10.1038/s41467-020-17928-5.
Souza-Filho, P.W.M., de Souza, E.B., Silva Júnior, R.O., Nascimento, W.R., Versiani de Mendonça, B.R., Guimarães, J.T.F., Dall'Agnol, R., Siqueira, J.O., 2016. Four Decades of Land-Cover, Land-Use and Hydroclimatology Changes in the Itacaiúnas River Watershed, Southeastern Amazon. J. Environ. Manage. 167, 175–184.
Tarpley, J.D., Schneider, S.R., Money, R.L., 1984. Global Vegetation Indices from the NOAA-7 Meteorological Satellite. Journal of Applied Climatology and Meteorology 23 (3), 491–494.
Torresani, M., Rocchini, D., Sonnenschein, R., Zebisch, M., Marcantonio, M., Ricotta, C., Tonon, G., 2019. Estimating Tree Species Diversity from Space in an Alpine Conifer Forest: The Rao's Q Diversity Index Meets the Spectral Variation Hypothesis. Ecol. Inf. 52 (July), 26–34.
Townsend, A., Asner, G., Cleveland, C., 2008. The Biogeochemical Heterogeneity of Tropical Forests. Trends Ecol. Evol. 23 (8), 424–431.
Turner, W., 2014. Conservation. Sensing Biodiversity. Science 346 (6207), 301–302.
Wang, R., Gamon, J.A., 2019. Remote Sensing of Terrestrial Plant Biodiversity. Remote Sens. Environ. 231, 111218. https://doi.org/10.1016/j.rse.2019.111218.
Wang, Y., Ziv, G., Adami, M., Mitchard, E., Batterman, S.A., Buermann, W., Marimon, B. S., et al., 2019. Mapping Tropical Disturbed Forests Using Multi-Decadal 30 M Optical Satellite Imagery. Remote Sens. Environ. 221 (February), 474–488.
Wortley, L., Hero, J.-M., Howes, M., 2013. Evaluating Ecological Restoration Success: A Review of the Literature. Restor. Ecol. 21 (5), 537–543.

Further reading

Sasaki, T., Ishii, H., Morimoto, Y., 2018. Evaluating restoration success of a 40-year-old urban forest in reference to mature natural forest. Urban For. Urban Greening 32, 123–132.